LAWRENCE
LIVERMORE
NATIONAL
LABORATORY

LLNL-BOOK-651958

Monte Carlo Simulations of Crystal Growth

L. A. Zepeda-Ruiz, G. H. Gilmer

March 19, 2014

Handbook of Crystal Growth, 2nd Edition

Disclaimer

Monte Carlo Simulations of Crystal Growth

Luis A. Zepeda-Ruiz

Physical and Life Sciences Directorate, Lawrence Livermore National Laboratory, Livermore, CA 94550

George H. Gilmer

Mechanical Engineering Department, Colorado School of Mines, Golden, CO 80401

Abstract

Atomistic models are advancing our understanding of crystal growth at an increasing rate, benefiting from rapidly increasing computational power. This chapter discusses Monte Carlo simulations that are focused on fundamental aspects film deposition on foreign substrates. The simulations demonstrate the influence on film nucleation and growth of the degree of wetting between the film and substrate, the substrate temperature, and the Ehrlich-Schwoebel barrier to diffusion over steps. Films grown with both de-wetting and an Ehrilch-Schwoebel barrier are often observed to form pinholes traversing the full thickness of the deposited film. Applications include (1) crystal growth issues involved in depositing films of uniform thickness with materials that have a propensity for de-wetting, forming three-dimensional islands; (2) device manufacturing involving thin films on topography such as trenches, minimizing the variation of film thickness; (3) controlling the morphology crystals in powdered molecular crystals.

Keywords: A1. Monte Carlo simulations, A1. Growth models, A1. Morphological stability, A1. Nucleation, A1. Roughening, A1. Crystal morphology, A1. Defects, A1. Diffusion, A3. Thin film, A3. Epitaxial growth, A3. Polycrystalline deposition

1. Introduction

In the last several decades, atomistic simulations have contributed enormously to our understanding of crystal growth mechanisms. In most cases, elucidating these mechanisms involves simulating the motion of a large number of atoms. Heavy computational power is required to bridge the gap between the atomistic length scale and mesoscopic regions that are large enough to accommodate the basic crystal growth mechanisms. An example is growth on a facet, requiring the nucleation of two-dimensional (2D) clusters. The computational cell must contain the critical nucleus and a region surrounding it sufficiently

large so that boundary effects are negligible. On one hand, the size of the critical nucleus depends on the driving force, and increases without limit as the driving force approaches zero. But deposition rates close to equilibrium can often be obtained by extrapolation from data obtained using higher driving forces. On the other hand, extremely high driving forces are often employed in magnetron sputtering chambers used in industrial manufacturing. In this case, the critical nuclei are small, but morphological instabilities often produce mounding and columnar growth structures that can reach sizes of several microns. A limiting factor with atomistic simulations is the efficiency of computers. During the last three decades the efficiency of computers measured in computations per kilowatt hour has increased by a factor of 10^4 [1, 2, 3]. Simulations that were impossible several years ago are now common at many universities and laboratories.

In this chapter we discuss physical vapor deposition (PVD) of crystals and films under a variety of conditions, using Monte Carlo (MC) simulations. We treat a small number of specific materials, but the mechanisms involved are often similar to crystallization phenomena observed in a large number of materials. Atomistic models of thin-film deposition and crystal growth have the advantage that the crystal lattice structure and atomic interactions are implicit in the models. For this reason, important phenomena such as faceting, grain-boundary grooves at growing surfaces, and polycrystalline microstructures are natural consequences of the simulations and do not require artificial constraints. Results of these models have played a central role in the understanding of the surface roughening transition and its effect on crystal growth kinetics. In addition, the influence of dewetting of films deposited on a foreign substrate, the formation of pinholes, have been successfully investigated using these simulations. In this chapter we review some of these applications and discuss MC modeling of sputter deposition of thin films based on materials parameters derived from first principles and molecular dynamics methods. Our models of deposition are large enough to exhibit clustered, columnar, and polycrystalline film structures. Applications to device fabrication are discussed based on simulations of film deposition onto substrates with topologies that includes vias and trenches, and their extension to the length scale of real devices.

The morphology of a thin film is influenced by the structure and properties of the substrate, the conditions that prevail during deposition, and transport properties such as diffusion rates on different crystallographic orientations. One of the most effective models that can match these diverse properties is based on MC simulations of kinetic lattice models. This approach has been used to study crystal growth and surface roughening on close-packed surfaces [4, 5, 6], the formation if 2D and 3D islands during the initial stages of film growth by PVD [7, 8, 9, 10, 11, 12, 13, 14], the columnar microstructure formed at low temperature PVD [15], and the trapping of defects, impurities, and of concentrations of the different species in a growing alloy [16, 17]. Complex crystals such as urea growth from solution have also been modeled using MD and MC simulations [18, 19]. This type of model has the advantage of fast computation because of the simplicity of the MC events, but at the same time it can include accurate rates

for atomic diffusion and other mechanisms based on more detailed simulations by MD or first principles methods (details of our implementation of the model are given in the bibliography [20]). The MD simulations can be used to obtain rates for processes that control and limit the growth process; diffusion rates, defect production, sputtering yields, and other information needed to match real materials. The book "Kinetic Processes", by K. A. Jackson has excellent discussions of MC modeling of the kinetics of crystal growth, together with experiments [21], and "Physics of Crystal Growth", by Pimpinelli and Villain treats theoretical aspects of crystal growth phenomena [22].

Most of the models developed to simulate the evolution of surfaces in three dimensions are based on continuum equations. Level-set continuum models are treated in a book by J. A. Sethian [23]. Models have been developed specifically for the morphology of step coverage for various amounts of surface diffusion and angular distributions (EVOLVE [24, 25]). The thickness of barrier layer films can be assessed by the use of these models, and this can be crucial for applications involving features with high aspect ratios; other continuum models are the level-set method [26], SPEEDIE [27], and the grain-growth model [28]. These models allow fast exploration of conditions, and are able to treat structure development on macroscopic length scales. Discrete atomistic and cluster models have also been applied to study issues related to metallization [29, 30].

Although the continuum models incorporate 3D features, complete simulations with microstructure development during growth including micro-voids and grain boundaries are dependent on data from atomistic modeling or detailed data from experiments. This is a difficult task because of the large number of parameters controlling mass transport, interface properties affecting wetting, and surface faceting. Atomistic models have the advantage that most of these parameters are implicit in the interatomic potential, and are not dependent on other simulations or experiments. An example of modifying a level-set model to treat bread-loafing correctly is discussed below in the section on deposition on substrates containing vias and trenches. Bread-loafing is the formation of a bulge overhanging the edges of trenches and vias; it is a universal result of low-pressure vapor deposition of thin films since it is caused the finite size of atoms. Bread-loafing can lead to void formation inside vias during the metallization step of silicon device fabrication. Also, stochastic effects of deposition and random nucleation events have not been included in most continuum models. For studies on this level of complexity, it seems appropriate to also apply atomistic models. After obtaining a detailed understanding of the atomistic processes, and some values for macroscopic parameters, the most important atomistic effects can often be included in the continuum models. Some processes are implicit in an atomistic model; for example, nucleation, statistical fluctuations in the deposition of atoms, and diffusion. The MC models require detailed energies for a number of atomic configurations, but recent improvements in first principles methods have enabled the development of good interatomic potentials for a large number of materials.

We discuss the application of MC models to faceting during growth, nucleation and growth during deposition of metal layers, and molecular crystals . In

particular, we describe the general aspects of our Monte Carlo model in Section 2. Section 3 treats some of the consequences of faceting during deposition. Sections 4 and 5 show the effect of materials properties and processing conditions on the nucleation and growth of films, respectively. Section 6 is concerned with the important issue of texture, and the influence of deposition conditions on grain orientation. Section 7 has a brief discussion of step coverage results. Finally, Section 8 describes some results for habit evolution of a molecular crystal.

This is a brief description of the method and a set of applications to crystal and film growth. We suggest that the reader goes to the references for a more detail of the examples shown here.

2. Monte Carlo model description

MC models of film deposition and crystal growth are based on the repetition of several basic events. In the general case, the simulation proceeds by selecting one of three events: (1) insertion of a sputtered particle (atom or molecule), (2) selecting a surface particle for a diffusion jump, or (3) evaporation. This type of model has the advantage of fast computation because of the simplicity of the MC events, while including accurate diffusion rates and other mechanisms based on more detailed data (i.e., MD or first principles calculations). Here we describe a basic form of the model; modifications of more complex systems are described below.

Deposition of particles on a substrate is accomplished by randomly selecting launching points in a plane above all occupied sites. Then, the particles are moved along the chosen trajectories in small increments until they reach a lattice site that has at least one occupied neighboring site. In cases where the site at the point of contact corresponds to an unstable position, the particle is moved to a stable site. Equilibrium deposition rate r^+ per surface site corresponds to zero driving force and is given by

$$r^+ = \nu \exp\left[-\left(E_g - E_k\right)/k_B T\right], \tag{1}$$

where E_g is the internal energy of a particle in the gas phase relative to that in the crystal, E_k is the energy of a particle at a kink site, k_B is the Boltzmann constant, T is temperature, and ν is an effective vibrational frequency. Note that the difference in free energy between a particle at a kink site and a particle in the gas phase, $(E_k - E_g)$, is the cohesive energy.

For the materials and temperatures we treat in this chapter, the deposition rate is typically many orders of magnitude larger than that of Eq. (1), and evaporation events can be neglected. Starting from an initial configuration, all particles are assigned to different lists based on their evaporation and surface diffusion rates. These lists are used to calculate a set of probabilities for picking a particle to execute an evaporation or diffusion event. The evaporation rate r_i^- and diffusion rate r_i^d depend on the number of nearest neighbors and are give by

$$r_i^- = \nu \exp\left[-\left(E_g - E_i\right)/k_B T\right] \tag{2}$$

and

$$r_{i\to j}^d = \nu \exp\left[-\left(E_i - E_j\right)/k_B T\right], \tag{3}$$

where E_i and E_j are the energies of the particles with i and j nearest neighbors, respectively. Now, the total event rate for the system is

$$R = \sum_i \left(N_i\, r_i^- + N_i\, r_{i\to j}^d\right), \tag{4}$$

where N_i is the number of surface particles in each of the i energy lists. Normalizing the weighted individual rates, r_i^- and $r_{i\to j}^d$, by the total event rate, R,

we obtain that an evaporation event is chosen with probability

$$P_i^- = \frac{N_i\, r_i^-}{R} \tag{5}$$

and a diffusion event (assuming a vacant neighboring site where the atom would have equal or lower potential energy)with probability

$$P_{i\to j}^d = \frac{N_i\, r_{i\to j}^d}{R}. \tag{6}$$

The elapsed time Δt, for an event attempted in a system with this set of N_i particles,is R^{-1},and the sum of these values for each event gives the elapsed time. The product of the elapsed time and the deposition rate determines the insertion of new atoms in the vapor.

A random number is used to select an event based on the above probabilities. After an event is chosen, a particle in that energy category is chosen, with a second random number, to perform the corresponding evaporation/diffusion event. When a diffusion event is chosen, a third random number is used to select a vacant nearest neighbor site. Finally, the corresponding energy categories are updated. Since surface diffusion events are chosen in a way that satisfies the condition for microscopic reversibility [4], a system evolving under surface diffusion alone will approach the equilibrium structure for the simulated temperature. Kinetic effects resulting from the deposition process become less pronounced for systems with a large surface diffusion mobility. The relative probabilities for selecting these events depend on the conditions being simulated. In particular, they depend on the ratio of the impingement frequency of sputtered particles to the hop frequency at the surface. A full description and variations of the MC model can been found elsewhere [20, 31].

3. Deposition on a spherical crystal seed

The early work using MC models has shown that close-packed surfaces in equilibrium tend to be atomically flat at low temperatures [32], provided that there are bond chains parallel to the surface orientation along two different directions [33]. This has consequences for the kinetics of crystal growth on these faces at low temperatures, since the generation of new layers on atomically flat surfaces requires the nucleation of stable 2D clusters of atoms. As is typical of nucleation processes, the growth rate on the surface drops exponentially as the driving force is reduced to small values. These results were observed in the MC simulations of the (001) face of a simple cubic Ising model [34, 32]. Because of the very low growth rate on the facet of a perfect crystal, deposition on different crystallographic orientations can be highly anisotropic. At higher temperatures, in equilibrium, the free energies of steps in the surface may drop to zero and the surfaces roughen. If this is the case for all close-packed orientations, the growth rate becomes nearly isotropic. This surface roughening transition has large consequences for crystal morphology, and for the morphological stability of surfaces during growth. As the temperature is increased the equilibrium density of steps increases until, at the transition temperature, the 2D islands percolate and form a connected structure across the entire surface. In this situation the growth rate is linear in the chemical potential driving force, since nucleation is not required.

3.1. Faceting during deposition of metals

The influence of crystallographic anisotropies on the growth of crystals is most clearly observed in the case of full three-dimensional (3D) systems in which all crystallographic orientations are accessible for deposition. For example, the fcc (111) and (001) orientations of Al crystals are atomically flat right up to the melting point, and only the (110) face exhibits a roughening transition [35]. Therefore we can expect some degree of faceting during growth on both the (111) and (001) faces at all temperatures.

The growth of an Al crystal with initial shape of a sphere is shown in Fig. 1. Starting from a spherical crystal seed that is 4 nm, as shown in Fig. 7 ,we inject atoms onto the crystal seed along the radial direction. The temperature was maintained at 200 K throughout the simulation. The initial sphere grows out to form an octahedron bounded by (111) faces. After the crystal reaches a critical size, the (001) faces appear, as shown in Fig. 1(b). The surface is covered with 111 and 100 facets, with 111 being dominant. Near equilibrium the 100 and 111 facets are comparable in size. However, the high adatom potential energy on the 111 surface causes it to become the dominant facet during growth. For the small initial sphere, the diffusion rate is sufficient for adatoms to diffuse to neighboring faces, and to congregate on the faces with the lower adatom potential energies. As a result, these faces can nucleate new layers and grow rapidly, until they disappear from the growth form, as shown in Fig. 1(c). Because of the small size of the initial sphere (4 nm initial diameter), there is little kinetic roughening induced by the deposition at the start. We found that 111 facets smaller than

about 12 nm in diameter are not able to nucleate new layers because the adatoms diffuse too quickly to the edges where they attach in sites of low potential energy such as step edges. As the crystal grows larger, the 111 facets reach the critical size, and multiple clusters can form. The steps from these clusters act as sinks for the adatoms impinging on the 111 face, so that fewer adatoms from these facets can reach neighboring 100 orientations. This effect slows the growth of 100 relative to 111 to the point that 100 facets remain on the growth form. This can be seen in Fig. 1(d).

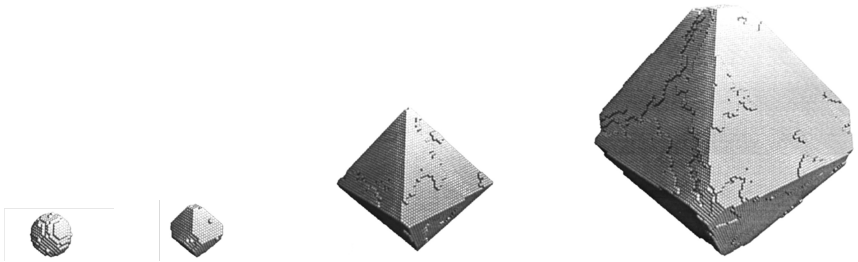

Figure 1: Simulation of deposition on a spherical seed of 4 nm diameter at 200K with a deposition rate of 1 μm/min. All particles are injected from a shell surrounding the crystal with velocities toward the crystal along the radial direction. Snapshots are taken at the start, (a); after deposition of 2×10^3, (b); after 5×10^4, (c), and after 5×10^5 atoms (d).

3.2. Effect of deposition rate

The effect of high deposition rates on the morphology of crystal formed by deposition on a small spherical seed is shown in Fig. 2. With increasing deposition rate, the facets shrink and eventually disappear. At the higher rates, there are not enough diffusion hops to move more than a few angstroms from the impinging point. Atoms that stick where they land tend to maintain the spherical shape. However, because of the small numbers involved, the fluctuations produce a rough surface, and as time goes on, a shadowing instability. A higher region on the surface intercepts more of the subsequent flux of atoms, and grows faster than its surroundings, which are being shadowed. This instability is an undesirable surface roughening mechanism.

Clearly the (111) facet will have a relatively small growth rate if most atoms arriving on it have time to escape to sites with lower energies. If the facet is sufficiently large, however, then there is time for other atoms to arrive and interact with others to form clusters. In this case, each atom is more likely to stick on the same facet close to the point where it arrived, and the growth would be less sensitive to crystallographic orientation. The transition from highly anisotropic growth (Fig. 1), to growth rates that are more nearly independent of orientation (Fig. 2) occurs at a critical facet radius R_c. A similar situation arises in the theory of kinetic roughening on "in finite" surfaces [22]. Rapid

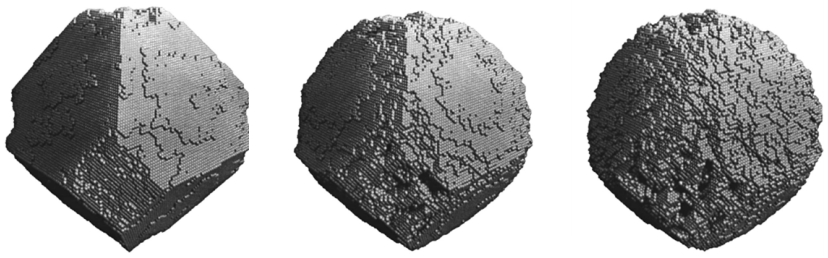

(a) (b) (c)

Figure 2: Comparison of deposited films on a spherical crystal seed as in Fig. 1; (a) with deposition rates of 10 μm/min; (b), 100 μm/min, and (c) at 1000 μm/min.

deposition onto close-packed orientations that are atomically flat in equilibrium will lead to some degree of kinetic roughening. This is a result of the nucleation and growth of the 2D islands. The average radius of atomically flat regions will have a magnitude approximately equal to R_c, since the flat regions larger than this value are likely to nucleate new 2D clusters and thus have their size reduced. This radius also gives a measure of the step spacing on a kinetically roughened surface. More information on how to calculate R_c can be found in Ref. [36].

4. Nucleation of films on foreign substrates

The early stages of thin film growth usually involve the nucleation of islands on a foreign substrate. Our purpose is to explore the influence of materials properties and processing conditions on cluster morphology. The initial islands have an important role in determining the initial orientations and density of the grains in the polycrystalline film [37]. For this purpose, we model the substrate as a single crystal, but with reduced interaction energies with the deposited material (the reduction being 0.15 eV per bond). In addition to having a reduced film/substrate bond energy, there is, in most cases, strain due to lattice mismatch which weakens the bonding compared to simple film/substrate bond energies. Furthermore, we explore the effect of temperature and inhibited diffusion at steps on cluster morphology. The latter was achieved by including different values of the Ehrlich-Schwoebel barrier (ϕ_{ES}), which assigns an extra activation energy for diffusion hops over a step edge for an adatom on the upper terrace [38, 39]. A large ϕ_{ES} inhibits adatoms from hopping into surface vacancy clusters and grooves, thereby slowing surface smoothening processes.

4.1. Effect of wetting

As a result of the difference in the interfacial energy between the film and the substrate there is a tendency for the deposited material to cluster and form islands form on top of the substrate. This effect is called de-wetting and is present in most film/substrate systems [40]. We will treat a system with weaker film/substrate interactions, and define the wetting parameter, w, as the ratio of the film/substrate interfacial energy to the film/film bonding energy ($w = [0, 1]$; 0 for homoepitaxy). Perfect wetting would require matching of both the substrate surface lattice spacing and inter-atomic forces to the film.

A comparison of clusters for different values of the wetting parameter is shown in Fig. 3. All three cases were produced by deposition of 2 monolayers of Be atoms with $\phi_{ES} = 0$ at a temperature of 20 °C. For the case of $w = 0$, Fig. 3(a) (perfect wetting), the clusters are thin and flat; as w increases, Figs. 3(b) and (c), they tend to be taller and, for the same amount of deposited atoms, cover less area. The voids between the 3D clusters resulting from strong de-wetting may initiate pinholes in the film that traverse the entire thickness. This is most likely to happen when the growth conditions are favorable for morphological instabilities. For example, a flux of atoms at grazing incidence, together with low mobility of atoms on the surface will deposit preferentially on the tallest clusters. This is an unstable process, since the taller clusters will intercept the most material and will grow faster shadowing more of the surrounding surface. A similar situation occurs if there is a significant barrier to cross over the steps, ϕ_{ES}; the lower surface regions are surrounded by steps going down, and the barrier impedes the filling in of this region by surface diffusion. This is called Schwoebel instability and is shown below. Figure 3(a) shows a simulation of deposition with perfect wetting. A large region of the deposited crystal is fully dense, whereas in Figs. 3(b) and (c) the deposited material have void regions starting at the interface with the substrate and extending a few

layers, clearly a consequence of de-wetting. The effect of de-wetting can be quantified by plotting the number of grains per layer vs. layer height. This is shown in Fig. 4 for the films shown in Fig. 3. Height = 1 correspond to the first layer above the substrate. Here we can see that the number of 3D clusters that nucleate and expand into grains during the early stages of deposition have a strong dependency on the wetting parameter w.

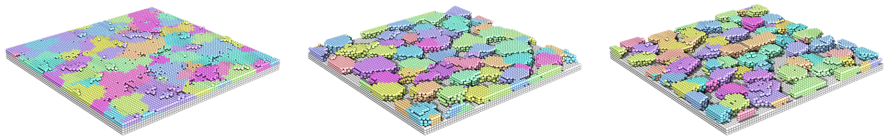

(a) (b) (c)

Figure 3: Comparison of cluster morphology during deposition of 2 monolayers (ML) of Be atoms at different values of the wetting parameter: (a) $w = 0$, (b) $w = 0.2$ and (c) $w = 0.4$. Other values are $T = 20$ °C and $\phi_{ES} = 0$.

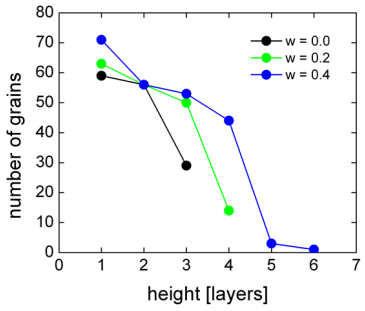

Figure 4: Plot of the number of grains per layer vs. layer height for the films shown in Fig. 3.

4.2. Effect of temperature

At higher deposition temperatures, the increased atom mobility reduces the number of grains as shown in Fig. 5. This is a result of increased ripening during deposition. The area of the substrate left bare increases with temperature, because of the diffusion of atoms from the substrate to the clusters, where a stronger bonding is favored. As can be seen from Fig. 6, the number of grains in all layers decreased a large amount in changing temperature from 61 °C to 145 °C.

4.3. Effect of inhibited diffusion over steps

Figure 7 shows the resulting morphologies after deposition of two monolayers (ML) of Be atoms at a temperature of 60 °C and the same wetting parameter

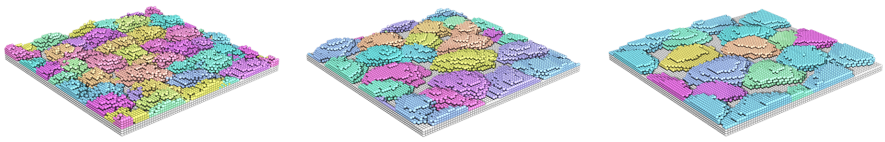

(a) (b) (c)

Figure 5: Comparison of cluster morphology during deposition of 2 monolayers (ML) of Be atoms at different temperatures: (a) $T = 61$ °C, (b) $T = 102$ °C and (c) $T = 145$ °C. Other values are $w = 0.1$ and $\phi_{ES} = 0.1$

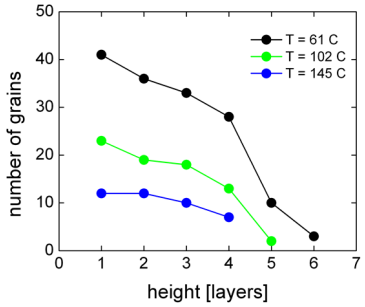

Figure 6: Plot of the number of grains per layer vs. layer height for the films shown in Fig. 5.

$w = 0.8$ but with different values of ϕ_{ES}. The effect of ϕ_{ES} on the surface morphology is evident. Most of the islands that have coalesced in the $\phi_{ES} = 0$ case have formed a flat surface, without steps or grooves at the grain boundaries (Fig. 7a). As the magnitude of ϕ_{ES} increases, more grain boundaries have developed grooves, resulting in a more disordered configuration (Fig. 7c). The increase in the number of grains (see Fig. 8) and surface roughness with increasing ϕ_{ES} occurs because of a reduction in the flux of adatoms from the upper terraces. This produces a greater probability to nucleate new layers on top of an island, and bias it to grow vertically instead of in the lateral directions.

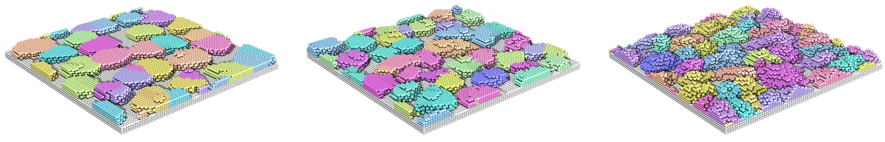

(a) (b) (c)

Figure 7: Comparison of cluster morphology during deposition of 2 monolayers (ML) of Be atoms at different values of the Ehrlich-Schwoebel barrier: (a) $\phi_{ES} = 0$, (b) $\phi_{ES} = 0.05$ eV and (c) $\phi_{ES} = 0.20$ eV. Other values are $w = 0.2$ and $T = 61$ °C.

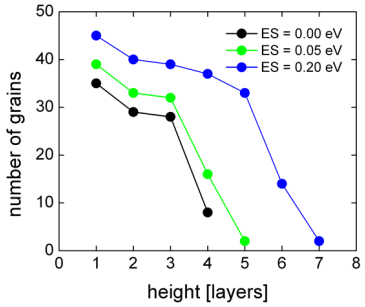

Figure 8: Plot of the number of grains per layer vs. layer height for the films shown in Fig. 7.

5. Film growth

The growth of uniform thin films on foreign substrates is impeded by several morphological instabilities. Hill-and-valley structures are formed and enhanced during sputter deposition where surface height perturbations have an opportunity to grow to large amplitudes [41]. While surface roughness can be partially controlled by changing growth conditions (such as deposition rate, substrate temperature, and angular distribution of impinging particles), the diffusion of particles over step edges plays a very important role in determining both surface roughness and the density of the films. During the initial stages of growth, each nucleation event creates an island with a random crystalline orientation. When two islands coalesce, grain boundaries are formed with reduced bonding between two atoms belonging to different grains.

5.1. Effect of wetting

As more atoms are deposited, and the clusters continue to grow vertically, some will attached to the lateral walls of the clusters, and will be stabilized by the strong film/film bonds. Eventually the clusters may coalesce completely with their neighbors, resulting in full density above this point. This depends on the degree of wetting, the Ehrlich-Schwoebel barrier (ϕ_{ES}), and the presence of grain boundaries. In Fig. 9(a) the film had a weak ϕ_{ES} barrier, but perfect wetting ($w = 0$). In this case, the region of the film close to the substrate has full density, without pinholes. The combination of ϕ_{ES} and grain boundaries has caused grooves to form after the deposition of several nanometers of material. The presence of a finite ϕ_{ES} inhibits atoms diffusing on the surface from filling the grooves. The formation of grooves is delayed until, (i) the deposited film is thick enough to have formed steps and, (ii) sufficient flux has crossed the steps to affect the growth on the downward sides of the steps. The grooves are located preferentially along grain boundaries, since the bonds crossing the boundaries are weaker as a result of the grain boundary energy.

The effect of de-wetting, Figs. 9(b) and (c), is to reduce the thickness of the region without pinholes and grooves, but the diameter of the columns is not

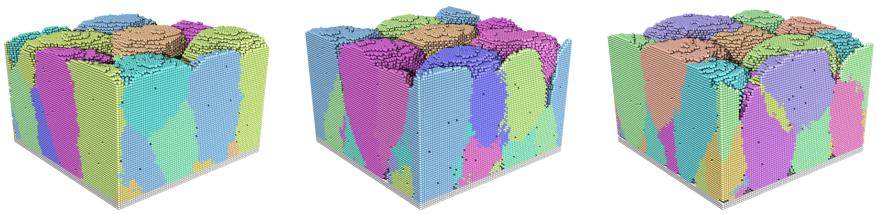

(a) (b) (c)

Figure 9: Simulated surfaces after deposition of 50 monolayers (ML) of Be atoms at different values of the wetting parameter: (a) $w = 0$, (b) $w = 0.2$ and (c) $w = 0.4$. Other values are $T = 60$ °C and $\phi_{ES} = 0.05$ eV.

sensitive to the degree of wetting. The magnitude of ϕ_{ES} is the primarily factor controlling the column diameters in this case. The grooves form closer together as ϕ_{ES} increases, since the downward flux across the step is reduced.

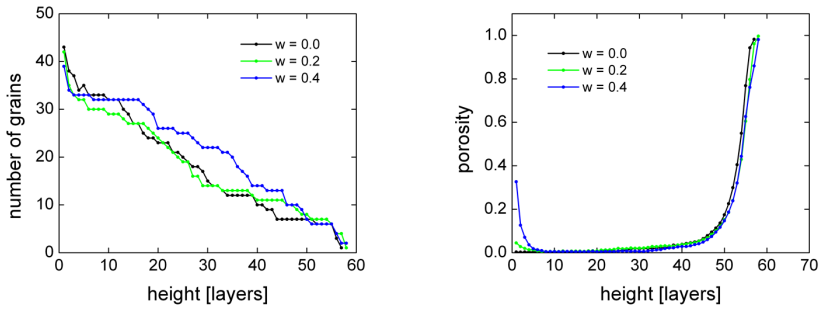

(a) (b)

Figure 10: (a) Number of grains vs. height and (b) Porosity for each crystalline layer after deposition of 50 monolayers (ML) of Be atoms for different values of the Ehrlich-Schwoebel barrier. In all three cases the substrate temperature is 200 °C and the wetting parameter is $w = 0.9$.

5.2. Effect of temperature

The effect of temperature in the film growth is illustrated in Fig. 11. The growth conditions, including the temperatures are the same as in Fig. 5, (showing the nucleation of the first two layers) except that the de-wetting parameter has been increased from $w = 0.1$ in Fig. 5 to $w = 0.3$. The stronger de-wetting is sufficient to produce pinholes extending through the entire film at all three temperatures. The effects of the higher temperatures are similar to those in Fig. 5; in that it increases the diameters of the columnar-shaped grains. However higher temperatures increase the densities of the films, whereas the densities in Fig. 5

are reduced. This seems to be a transient effect during the initial growth, where high mobility causes atoms to diffuse to the higher levels and thereby to increase the height of the clusters at the expense of their girth.

The tops of the columnar grains become flat, with only a few steps at the higher temperatures. Again, this is very similar to the clusters in Fig. 5. At the lowest temperature, the nucleation of a 2D island on top of the surface requires only few atoms, and the density of the 2D islands is high, producing a rough top to the columnar grains. The larger diffusion coefficient of adatoms, and the large critical nucleus greatly decreases the density of stable 2D islands.

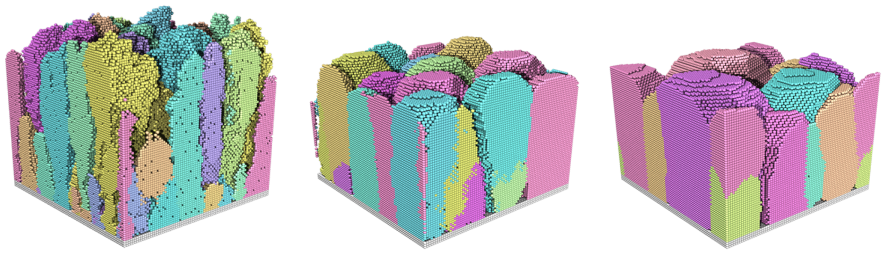

(a) (b) (c)

Figure 11: Simulated surfaces after deposition of 50 monolayers (ML) of Be atoms at different temperatures: (a) $T = 61$ °C, (b) $T = 102$ °C and (c) $T = 145$ °C. Other values are $w = 0.3$ and $\phi_{ES} = 0.10$ eV.

The number of grains in 2D horizontal layers is given in Fig. 12, as a function of the height of the layer. The values for the lowest temperature (61°C) deposition are much higher than those for the two higher temperatures.

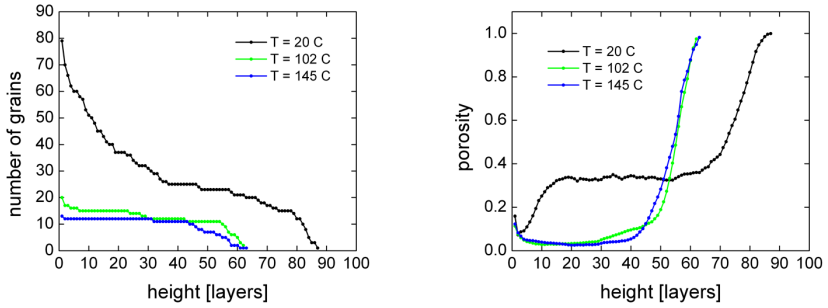

(a) (b)

Figure 12: (a) Number of grains vs. height and (b) Porosity for each crystalline layer after deposition of 50 monolayers (ML) of Be atoms for different temperatures, from configurations in Fig. 11. In all three cases the Ehrlich-Schwoebel barrier is $\phi_{ES} = 0.10$ eV and the wetting parameter is $w = 0.9$.

5.3. Effect of inhibited diffusion over steps

Further growth of a film beyond the first few monolayers shows that ϕ_{ES} also has a strong effect on the morphology in this regime. Figure 13 shows three different films obtained after deposition of 50 ML of Be atoms at a temperature of 200 °C, a wetting parameter $w = 0.9$ and $\phi_{ES} = 0$, 0.05 and 0.15 eV in (a), (b), and (c), respectively. In the case where $\phi_{ES} = 0$, a smooth surface forms, with only a few steps surrounding two-dimensional islands (Fig. 13a), as expected for layer-by-layer growth. On the other hand, the $\phi_{ES} = 0.05$ eV case shows deep grooves, even with a relatively small barrier (Fig. 13b). Note that the grooves developed during deposition may not extend all the way down to the substrate. This can be seen in the plot of porosity vs. height of Fig. 13(c). We defined porosity as the number of vacancies at each layer of the film normalized to full coverage. In the simulations shown in Fig. 13(a) and (b) we use an almost perfect wetting between the film and the substrate ($w = 0.1$). This results in a fully dense film (0 porosity) close to the substrate since the Ehrlich-Schwoebel instability requires some time to develop and to produce the grooves that cause the reduction in film density. Approximately a 25% reduction in density is produced with $\phi_{ES} = 0.15$ eV, after the initial transient. Even the film with $\phi_{ES} = 0.05$ eV shows some signs of reaching a steady state reduction of several percent in density. Further growth would be required to confirm this. Increasing ϕ_{ES} of Fig. 13(b) from 0.05 to 0.10 eV, and strengthening de-wetting, from $w = 0.1$ to 0.3, as in Fig. 11(c), results in pinholes that penetrate through the film to the substrate, as shown in Fig. 14. Methods to control these pinholes are important for controlling the magnitude of stress in the film [42].

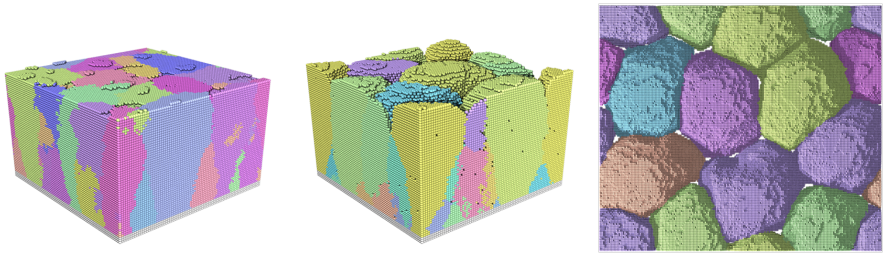

(a) (b) (c)

Figure 13: Resulting surfaces after deposition of 50 monolayers (ML) of Be atoms at different values of the Ehrlich-Schwoebel barrier: (a) $\phi_{ES} = 0$ and (b) $\phi_{ES} = 0.05$ eV. (c) $\phi_{ES} = 0.15$ (top view). Other values are $T = 145$ °C and $w = 0.1$.

5.4. Strategy to grow a smooth film

Temperature has a well known effect on thin film morphologies, i.e., a low-density irregular columnar microstructure is formed at low temperature where the impinging atoms do not have sufficient mobility to diffuse more than a few

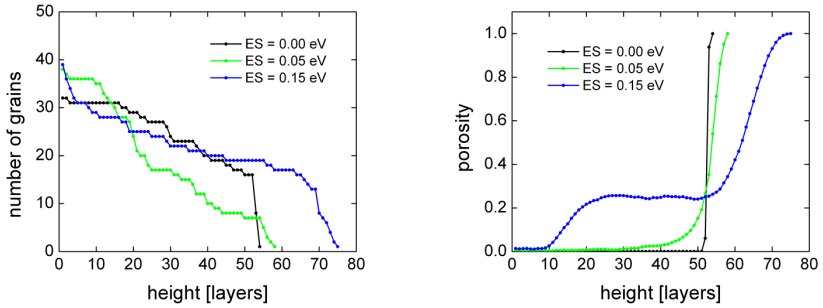

(a) (b)

Figure 14: (a) Number of grains vs. height and (b) Porosity for each crystalline layer after deposition of 50 monolayers (ML) of Be atoms for different values of the Ehrlich-Schwoebel barrier from configurations in Fig. 13. In all three cases the substrate temperature is 200 °C and the wetting parameter is $w = 0.9$.

Ångstroms from the point where they contact the surface. This effect is crucial for the processing of metallic interconnects in the silicon device manufacturing industry. Pore formation will create non-uniform film thickness and regions likely to fail during device operation.

Our MC simulations show that the uniformity of a non-wetting film may be improved by depositing the film at two temperatures. When a few monolayers are deposited with a low substrate temperature, as shown in Fig. 15(a), surface diffusion rates are small, and atoms stick close to the point where they impinge. A dense array of small 3D islands are formed and coalesce. Once percolation occurs, the 3D islands form single connected layers, with low density and containing Ångstrom sized pores, extending through the film. As shown in Fig. 15(b), increasing the temperature does not improve things, since the extra mobility causes de-wetting of the film from the substrate. As the initial atoms are deposited on the substrate, they diffuse and cluster together to form small islands that grow vertically because of the stronger bonding of the Al atoms with other Al atoms than those between the Al atoms and the substrate. This causes them to grow into large 3D islands, with bare substrate between them.

Our method will take advantage of the low temperature deposition to prevent the deposited atoms from forming 3D islands, and yet provide mobility to to fill the small pores that form at the low temperature, we can deposit a few layers at 175 K, and then once percolation occurs, increase the substrate temperature to 250 K so that the atoms in the film are mobile. Then the deposition is continued until the desired thickness is obtained. The initial uniform film is metastable against de-wetting, since the small holes in the percolated film will fill in because of the negative curvature of the holes and it provides a perfect wetting surface for the high temperature deposition. The simulation can provide information on the optimum values of the parameters (e. g., the temperatures) for formation

(a) T = 175 K

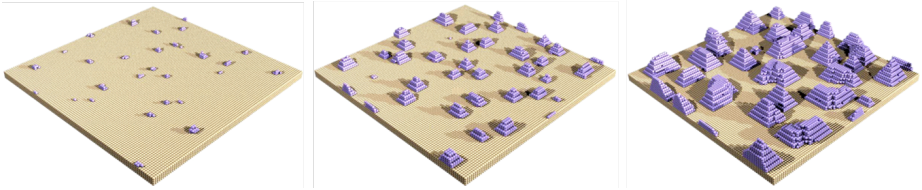

(b) T = 250 K

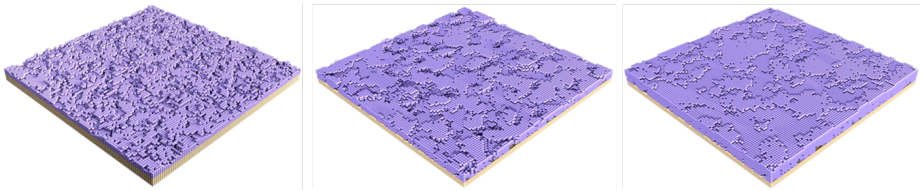

(c) T = 175 K (first image) and then T = 250 K

Figure 15: Control of substrate temperature during deposition is used to obtain uniform Al film on a plastic substrate. (a) Deposition on substrate at 175 K, (b) deposition on substrate at 250 K, and (c) initial deposition with substrate at 175 K, and continued deposition at substrate temperature of 250K.

of a smooth film.

6. Texture development

One of the most important aspects of the growth of polycrystalline films is the tendency for the grains to develop a preferred orientation. This occurs even in the case of amorphous substrates, and is therefore not likely to result from atomic alignment or 'template' effects at the substrate-film interface. In most cases a particular crystal axis of the grains is aligned within a few degrees of the normal to the plane of the substrate. In-plane crystal axes are generally rotated in random directions, although in some cases there are more low-angle grain boundaries than would be present for random in-plane orientations.

A number of mechanisms have been proposed to explain the appearance of texture, but most apply to growth at relatively high temperatures. In that case, high atomic mobility is thought to permit the expansion of grains oriented in such a way as to minimize either strain energy or surface energy [43, 44]. Texture in refractory materials is thought to be a result of competitive growth; crystallites oriented with a fast-growing surface parallel to the substrate will incorporate a disproportionately large fraction of the deposited atoms, and eventually encompass the grains with slower growing surface orientations. Some materials such as TiN can exhibit different textures if the conditions are changed. At room temperature, TiN grows with the fast-growing (111) face parallel to the substrate, but at 800 V the texture is that of the slow-growing (001). This change also occurs at room temperature if a beam of low-energy ions is directed toward the surface, thus increasing the mobility of the surface atoms [45]. This change is thought to be a result of the high mobility, since the surface energy is reduced.

We first consider the deposition of Al at 100 K. At this temperature only adatoms on (111) faces have high mobility because of their small activation energy (0.08 eV) for diffusion. Some configurations generated by the model during the initial growth of the film are shown in Fig. 16. Crystallites with (001) faces parallel to the substrate normal have much higher 2D nucleation rates than those with (111) parallel. This is result of a higher adatom potential energy on the (111) faces, resulting in lower adatom concentrations. Rapid 2D nucleation causes faster vertical growth rates on the (001) surfaces. These crystals to grow higher, and because of their height they intercept more flux than do the (111) oriented crystals, resulting in even faster growth. As the film grows thicker, the (001) crystals dominate, although the region near the substrate has both orientations present.

Fig. 17 shows the film during growth at a temperature of 300 K, were the mobility is much higher. In this case the crystallites with the larger lateral growth rate dominate. The density of clusters is lower because of Ostwald ripening; at the higher mobility small clusters will dissolve and supply larger, more stable clusters. Adatoms on the (111) face can diffuse even farther and stick preferentially at the edges of the cluster. As a result, the (111) grains spread laterally over larger distances. The (001) grains are again higher and intercept moreflux, but in this case the higher mobility allows significant atomic exchange between (001) and (111) grains. Because of the higher radius of curvature of the (001)

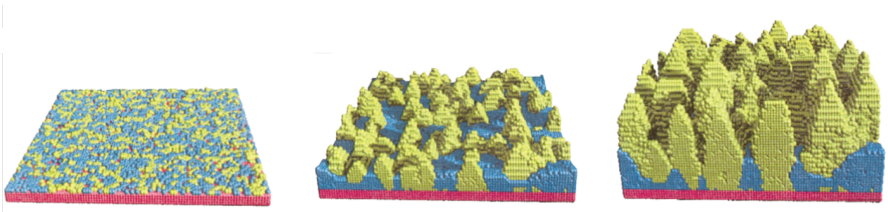

(a) (b) (c)

Figure 16: Simulated growth of Al deposited at 1μm/min at a temperature of 100 K onto a flat substrate, and with a cosine angular distribution for the impinging Al atoms. Clusters with (001) and (111) are permitted to nucleate and grow simultaneously using the multi-lattice model. The substrate is dark grey, the (111) clusters an intermediate shade, and the (001) clusters are light grey. Configurations (a), (b), and (c) correspond to the film at different times during the deposition.

crystals (smaller cross-sections), they have a higher chemical potential and loose material in the exchange. This loss of material is greater than the gain resulting from the height advantage of the (001) crystals, and as a result the (111) crystals eventually cover the entire surface of the film.

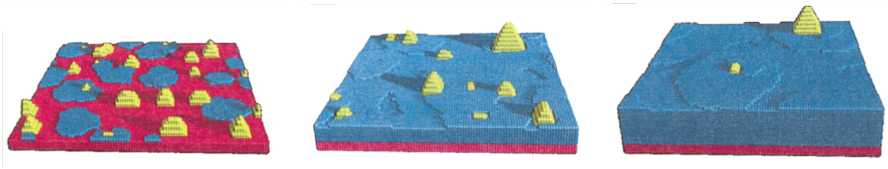

(a) (b) (c)

Figure 17: Simulated growth of Al deposited at 1μm/min at a temperature of 300 K onto a flat substrate. The angular distribution is cosine, and the cluster orientations are indicated as in Fig. 16.

The flux to the (001) oriented crystals, relative to those at other orientations, can be altered by changing the angular distributions of the impinging atoms. Atoms arriving at oblique angles to the substrate are most likely to strike one of the higher crystals, whereas atoms arriving at normal incidence should impinge on (001) and (111) crystals with equal probability. Thus, the use of a collimator would be expected to reduce the growth rates of (001) crystals more than the (111). To test this conjecture, we examine the result of collimated growth under low mobility conditions. This is shown in Fig. 18. Only the angular distribution is changed from the simulation shown in Fig. 16. It is apparent that the amount of material with (111) texture is considerably thicker than in the un-collimated case. The angular distribution of the impinging atoms clearly has a large effect on the film structure, and at a somewhat higher temperature, it can make the

difference between depositing films of (111) or (001) texture. Film texture has a strong effect on the density of thin films of refractory materials, and methods to control texture have important technological applications.

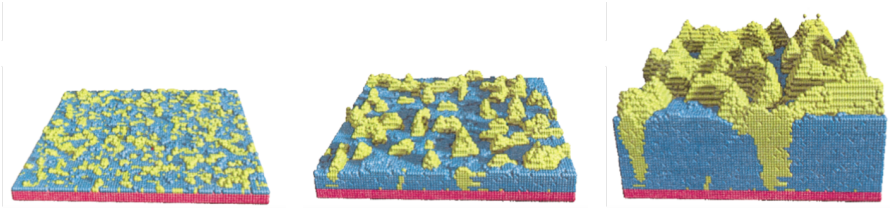

(a) (b) (c)

Figure 18: Simulated growth of Al deposited at 1μm/min at a temperature of 100 K onto a flat substrate. The angular distribution is cosine as modified by a 1:1 collimator.Cluster orientations are indicated as in Fig. 16.

7. Physical vapor deposition and step coverage

Thin films of metal are a crucial part of current on-chip interconnection technology. The films serve as diffusion barrier layers; e.g., Ta and Ti, and seed layers of Cu, among others. These layers are typically deposited over substrate topography for integrated circuit fabrication, using low pressure magnetron sputtering. The step coverage on trenches and vias is usually the region of minimum film thickness inside a feature, and this thickness is a key quantity that indicates the future integrity of the layer. Both surface tracking and atomistic models have been applied to treating this important step in fabrication of devices [46, 47, 9, 48].

Although continuum models are used extensively in the software employed in the fabrication of electronic devices, these models have serious shortcomings. The surface evolution resulting from the deposition of discrete particles is intrinsically different from that produced by continuum processes. The atomistic effects have major consequences, even when observed at macroscopic length scales. The MC model represents the physics of the deposition process a great deal more faithfully than the continuum model. Monte Carlo codes can fairly easily be used to simulate the kinetics of surface impingement and are, by their nature, stochastic.

An interplay between continuum and atomistic simulation approaches led to the development of a continuum model that mimics a key mechanism that is represented in the atomistic model but absent in the usual continuum model. It turns out that the effect is quite pronounced in certain cases, namely collimated and low energy ionized PVD. In these regimes of deposition, the film can exhibit a "catastrophic" shadowing instability at the upper corners of the feature profiles, leading to exceedingly low film coverage at these locations. The usual continuum model almost completely fails to capture this phenomenon, thereby undermining confidence in its predictions of minimum step coverage under these deposition conditions. The MC model, on the other hand, does reproduce the behavior observed in experiments.

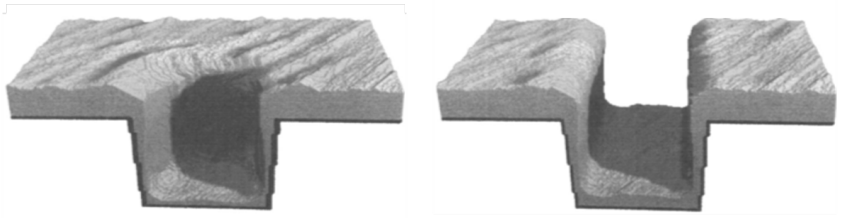

(a) (b)

Figure 19: Configurations generated by the MC model with a substrate containing a 0.025 μm (a) via and a(b) trench. Here the temperature during deposition was held at 390 °C, and the deposition rate was scaled to correspond to 0.25 μm/min for a 1 μm trench (the actual deposition rate was 1.6×10^4 μm/min).

Films simulated by the MC model of deposition onto a via and a trench are shown in Fig. 19. The thickness of the deposit in the bottom of the via is greater than that of the trench. This results from the fact that the via walls shadow the center more effectively. Trajectories of atoms arriving at large angles of incidence are all blocked and can not reach the bottom of the via, whereas some large angle trajectories arriving at the trench can reach the bottom. The high temperature 390 °C redistributes the sputtered material by surface diffusion, and for this reason the overhang produced by the breadloafing effect is not as large as that typically observed during manufacturing. Note that the thinnest film on the sidewalls is at the bottom, a characteristic of high surface diffusion. The name "breadloafing" is derived from the shape of baked bread rising out of the pan and bulging out over the edges.)

An experiment showing more pronounced breadloafing was performed, with deposition at room temperature of a Ta layer on a substrate containing vias, and is shown in Fig 20. The mobility of Ta at room temperature is extremely low and as a result, the thickness increases with depth, just the opposite of Fig. 19. The overhang expands with the amount of material deposited, blocking a region on the sidewalls that increases with further deposition. This gives rise to the taper of the sidewall film, that decreases in thickness with height. At the corner the sidewall thickness is essentially zero, since that region is blocked with the initial film deposition. The sputter gas was Ar at a pressure 1 mTorr and no electrical bias was applied to the substrate. A scanning electron micrograph of one deposition is shown in Fig. 20,(b). A corresponding simulation is shown in Fig. 20,(c). The throw distance is 10 cm while the target diameter is 6.35 cm. Hence, at low pressure where there is negligible scattering, the flux at the substrate is confined to a cone of angles less than 18 °; a moderately collimated beam. The agreement of the standard levelset model with the experiment is poor, with only a slight bulge where the experiment shows a large overhang. The sidewalls have uniform thickness in the levelset model, whereas the experiment shows a taper with the thick region at the bottom of the via.

In Fig. 20(b) we see three important features of the film morphology. First, the sidewalls exhibit a highly columnar microstructure. This is a consequence of the high angles of incidence of the largely collimated flux of Ta together with the extremely low surface mobility of Ta. Second, the film appears to be fully dense on those parts of the via that are approximately normal to the incident flux, namely on the bottom of the via and on the field. The film in these places is very smooth which is a consequence of the almost-normal incidence but also perhaps because of the energy of the impinging atoms. The energy of the sputtered Ta is 25 eV on average. Third, the minimum step coverage occurs at the upper end of the sidewall rather than the more usual location at the bottom of the sidewall in less collimated deposition. Immediately above this "pinched" region the film bulges sideways forming an almost semicircular overhang. The overhang shadows the wall from the collimated beam, and causes the pinch at the upper sidewall.

The drastic difference between the experiment and continuum model can be understood by the crucial difference between the behavior of particles of an

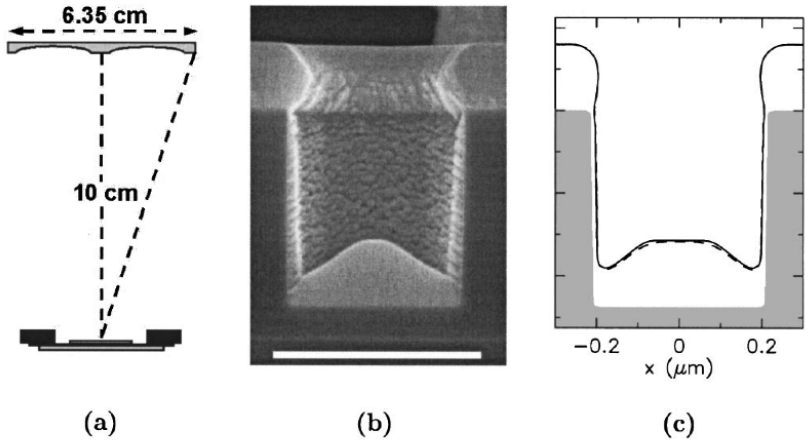

Figure 20: (a) Sketch of Ta deposition experiment. (b) Cross-sectional scanning electron micrograph of an axis symmetry contact via with Ta barrier layer. Dark areas indicate SiO2 substrate and light areas indicate Ta. Via depth 460 nm, width at top 430 nm, width at bottom of via 415 nm, scale bar is 500 nm wide. (c) Numerical simulations using continuum model. Solid line: ballistic deposition with cosine angular distribution from target. Dashed line: simulation utilizing angular distribution obtained from gas scattering code, mean free path 5 cm.

atomic flux, and that assumed in the continuum model. This difference affects the shape of thin films in a number of different applications. Fig. 21 shows a schematic comparison of atomistic with continuum models.

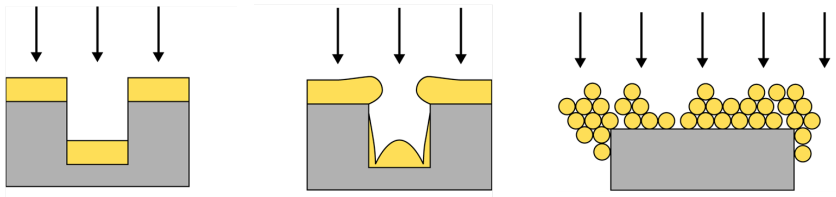

Figure 21: Schematics showing: (a) a film deposited on a trench simulated by a continuum model, compared to (b) a typical MC simulation of a film resulting from a collimated beam of atoms, and (c) a diagram from MD simulations indicating how atoms extend over the edge. As the film grows thicker, it extends farther at the overhang. This angle is independent of the atomic size.

Each segment of the film surface is assumed to receive a flux from the source(s) that are visible from the source, corrected for the orientation of the segment relative to the direction of the source. The collimated flux therefore has no interaction with the vertical walls, in the schematic Fig. 21(a) . (Numerical

errors cause a small amount of material to attach to the walls in Fig. 20(c).) But the particles in Fig. 21(b) will not simply slide down the vertical walls, if they come within an atomic interaction range of the walls. Some of the particles will stick on the wall just because they are within several Ångstroms of the wall. Also, particles that impinge near the edge of the trench will diffuse diffuse over the corner and find stable sites on the vertical walls, as illustrated in Fig. 21(c). Although the deposition of a single layer of particles will not cause significant overhanging material, the second layer will, on the average extend farther out over the via by a distance proportional to the atomic diameter. A film will extend out in Angstrom sized increments as each layer is deposited, and will extend out a distance proportional the film thickness. This overhang is essentially zero for the continuum model, no matter what film thickness is deposited, but it may be significant for particles.

Although the discussion has assumed that the film thickness is only a fraction of the diameter of the via, or the trench width, there are applications where the deposited material is expected to fill the via, and therefore a layer is deposited that is at least as thick as the via diameter or trench width. In this case, the overhangs of the breadloafing effect can coalesce from both sides of the trench (or via) and seal off a void. Again, the continuum models are unable to predict the occurrence of void creation, although they may have a deleterious effect of the long-term performance of the device.

Other applications where continuum modeling yields erroneous results are illustrated in in Fig. 22. A shadowing instability can produce low-density porous material; one example where low diffusion coefficients and the flux of atoms impinging at a glancing angle is the deposition on the sidewalls of the via of collimated Ta, mentioned above, Fig. 22(b). Again, there is a large difference between the morphology predicted by a continuum model and an atomistic model. In most cases the continuum models predictions are more favorable to the application than the real atomic flux. Finally, deposition of piezoelectric films onto a substrate containing an electrode leaves a gap between the electrode with a film on top and the film on the substrate, as shown in Fig. 22(c).

We have developed a continuum model that incorporates finite atomic length scales. The model incorporates effects of atomic interactions, which lead to the capture of impinging atoms that pass near a point on the film. The effect of this capture process results in breadloafing at corners and convex regions of a surface with large curvature. The model employs the same calculation for the flux and its interaction with the surface of the substrate or film, but includes a calculation of the distance between the atoms flux from all sources, but instead of requiring that the flux impinge on a surface, it is can also contribute to surface regions in close proximity to the path of the flux. The results for deposition onto a via are shown in Fig. 23. This model does not take into account the details of the atomic displacements on collision with a surface, but it does detect situations where impinging particles would come within the capture radius of the film, causing them to stick.

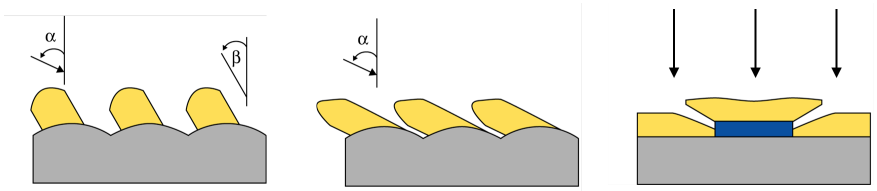

(a) (b) (c)

Figure 22: Atomic size affects the morphology of the deposited film on a macroscopic length scale; each layer of atoms deposited extends in the same direction, so the displacement accumulates. Here α is the incident angle of the atoms in the beam, and β is the average angle of the columns. (a) A schematic of columns formed by atomic beams; experiment or MC atomistic simulation, (b) schematic of columns simulated using levelset continuum model. (c) Typical piezoelectric film deposited onto an electrode in a filter arrangement in a cell phone. The material deposited on top of the electrode is not connected to the film on the substrate.

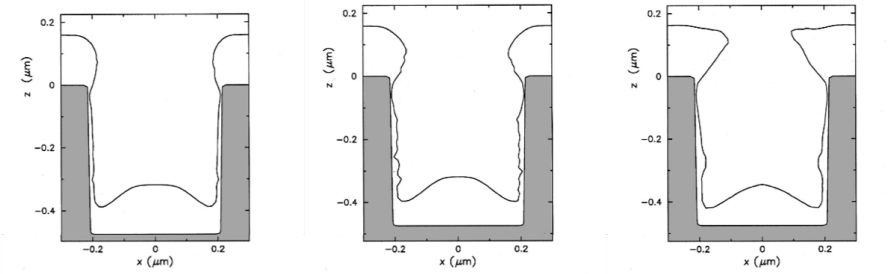

(a) (b) (c)

Figure 23: Cross-sectional views of sputter deposition into axisymmetric contact vias corresponding to the modified level set model. Capture distances are 5, 20, and 120 Å.

8. Size and habit evolution of molecular crystals

The size and shape distribution of crystallites controls important materials properties, such as chemical, mechanical, thermal, and optical properties that can be quite different from the bulk. It is therefore not surprising that many studies exist in the literature, both experimental and theoretical, of how crystallites grow and change shape and how such evolution is affected by external factors like stress, temperature, solvent, additives and so on [49, 50]. General theories for predicting crystal morphology based on considerations of geometry [51, 52], surface free energy [53], and attachment energy [54, 55, 56] have been around for several decades. Using empirical inter-atomic potentials such theories have been used to predict the "average" morphology of crystallites belonging to a wide variety of materials types: metallic, semiconductors, ionic, organic, etc. However, such approaches yield morphologies where kinetics are included only in a very approximate way. Real systems typically consist of a

distribution of crystallite shapes and sizes. For an understanding of how such a distribution depends on various external factors, it is desirable to create a simulation method that takes important kinetic processes into account, such as the ratio between diffusion and incorporation of molecules.

A typical PETN (Pentaerythritol Tetranitrate) crystal is shown in Fig. 24(a). Although this crystal was grown from solution, it exhibits the primary facets that are observed during growth from the vapor. This crystal was grown by slow recrystallization from acetone yielding colorless crystals at 4 °C and have an average aspect ratio of 5:2 for the length:width. Figure 24(b) shows the predicted growth morphology or crystal "habit" of a PETN crystal obtained by a standard Wulff construction but using the so-called attachment energies instead of surface free energies [54]. A Wulff construction based on the surface free energies yields the equilibrium morphology, which for the PETN crystal looks very similar to the growth morphology of Fig. 24(b) and therefore is not shown. In the computed morphology, the crystal habit matches the experimentally grown crystal of Fig. 24(a), where four {110} facets are shown along the length (long axis), while the end caps are facetted by eight planes belonging to the {101} family. However, most of the experimental particles deviate from the nice symmetry of Fig. 24(b).

These solution grown crystals are compressed to 50% of its theoretical maximum density and the resulting powder is stored for several years. At room temperature the powder is stable showing no rearrangement over a period of several days. The rate of recrystallization and the aspect ratio of the crystallites are strongly dependent on the temperature at which the PETN is kept. The change in aspect ratio may result by changing the supersaturation of the environment where the PETN powder is maintained. Although the particle size distribution can be measured experimentally, there is little information on the mechanism associated with the change in surface area. The resulting morphology during aging also appears to be dominated by the two families of facets shown in Fig. 24(b). Figure 24(c) is a SEM micrograph of PETN crystallites resulting from subliming PETN powder followed by aging at 80 °C for 90 days at ambient pressure. These crystallites in Fig. 24(c) show a clear propensity for elongation along the $\langle 001 \rangle$ axis, with aspect ratio in excess of 100:3 for some of the crystallites. Although crystallites are elongated along the crystal $\langle 001 \rangle$ axis, the ratios of surface area of the {110} to the {101} facets vary significantly from crystallite to crystallite and the areas of the end {101} faces are typically unequal within the same crystallite.

For this study, we substitute the entire PETN molecule, $C(CH_2ONO_2)_4$, by a single unit whose interaction depends on its local environment, i.e., number and type of neighbors. This allows us to substitute the complexity of the 29 atoms that form a PETN molecule by an equivalent unit that is packed on a body center tetragonal lattice [31], and to study the unit-unit interaction on a lattice in a manner similar to crystal graph theory of Hartman-Perdok [54]. Starting from a given initial configuration, each MC step consists of choosing a particle at random and moving it to a randomly chosen unoccupied site within a given cutoff radius. Next, we calculate the change of energy, ΔE,

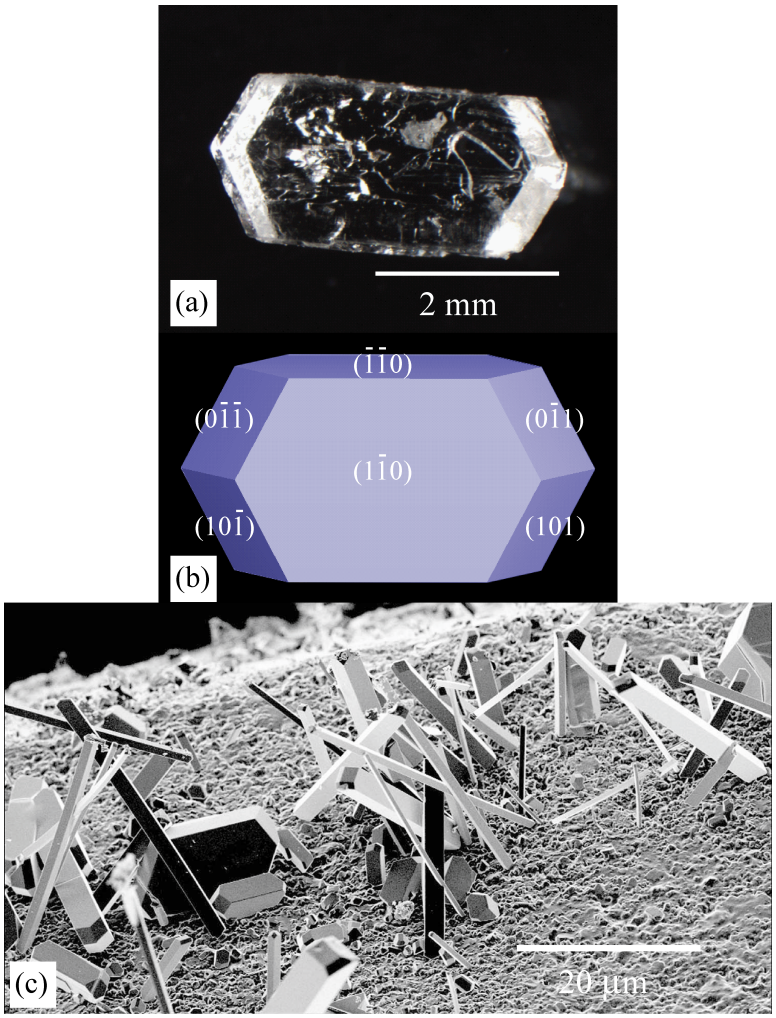

Figure 24: (a) Microscope image of a typical PETN crystal grown from solution. (b) HartmanPerdok (HP) growth morphology of PETN as computed by the COMPASS forcefield via the attachment energy method. Two types of facets are prominent, four elongated faces of the {110} family and eight end faces of the {101} family. (c) Microscope image of typical PETN crystallites illustrating a variety of aspect ratios after aging.

due to this move. The new configuration is accepted with probability 1 if the resulting energy change ΔE is less than zero, and accepted with a probability $\exp(-\Delta E/k_B T)$ otherwise. This local random walk can be interpreted as the result of a few successive neighboring hops. Such procedure ensures that all possible configurations can be sampled. Also since all attempted atomic displacement steps obey detail balance it implies that the system approaches an equilibrium configuration as the simulation time approaches infinity. A more

accurate simulation of the kinetics of the morphology evolution would involve neighboring diffusional steps weighted by factors determined by the activation barriers and changes in energy. This would require the calculation of a large number of possible diffusion pathways, the corresponding transition states, and hopping rates.

The influence of crystallographic anisotropy on the growth and evolution of PETN crystals is most clearly observed in the case of a full three-dimensional system in which all crystallographic orientations are accessible for diffusive transport. As a first step in our analysis of size and habit evolution, we decided to study the evolution of the shape of a PETN crystal starting from an arbitrary initial shape. Fig. 25(a) displays the specific example of a spherical crystallite of diameter 16 nm, which was equilibrated for 2×10^6 MC steps. The reason for choosing a sphere was to eliminate any directional bias or artificial anisotropy that might influence the resulting crystallite shape. The resulting configuration, Fig. 25(b) shows the presence of 101 and 110 facets, also present in the Hartman-Perdok predicted morphology. In addition, four small 100 faces are also present. Note the comparable surface energies (obtained by COMPASS calculations) between these 3 faces: 0.21, 0.27 and 0.27 kcal/(molÅ^2) for the 101, 110, and 100 surface, respectively. Thus, the appearance of these facets in the equilibrated structure gave us confidence not only in the accuracy of the inter-molecular lattice potential, but also its ability to mimic realistic crystallite shapes when used with the MC procedure described above.

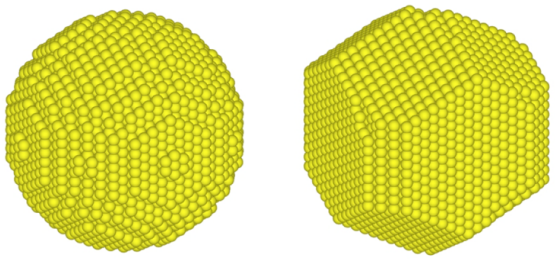

(a) (b)

Figure 25: Resulting equilibrium configuration obtained from a spherical PETN crystal of 16 nm in diameter that was annealed for 2×10^6 MC steps.

The morphology in Fig. 25(b) results from the "local rearrangement" of a fixed number of particles (the ones that formed the initial spherical crystallite) driven by the tendency of the system energy to reach a local minimum. However, the experimentally observed morphologies are a result of growth through particle addition and diffusion, whose rates strongly depend on experimental conditions. To this end, we have studied the change in morphology during growth in a similar way as described in Ref. [20]. Thus, we start from an initial spherical seed, and add particles to the surface of the growing crystallite along a randomly

selected radial direction. Following each particle addition we perform a predefined number of MC steps, aimed at representing surface diffusion. Thus the above number of MC steps between two successive particle addition events represents, on an average, the ratio of the diffusion hop rate to the crystallite growth rate.

Figure 26 shows the evolution of an initial spherical seed of 5 nm in diameter at 300 K. We performed 17 MC steps per insertion and particles were allowed to move within a cutoff radius of 5 nm. After insertion of only 200 particles, as shown in Fig. 26(a), the surface of the crystal is bounded by 101 and 110 facets of approximately the same size. As more material is added to the crystal, 110 facets become dominant as shown in Fig. 26(b). This is a result of the difference in adatom potential energy between these two faces. The 101 faces have a lower adatom potential energy (-28.7 kcal/mol) than the 110 faces (-18.7 kcal/mol), thus making the nucleation of a new layer easier and leading to a faster growth, as shown in Fig. 26(c). As the crystal grows larger, the 110 facets can nucleate stable two dimensional islands that allow these faces to grow through the motion of monatomic steps, as shown in Fig. 26(d).

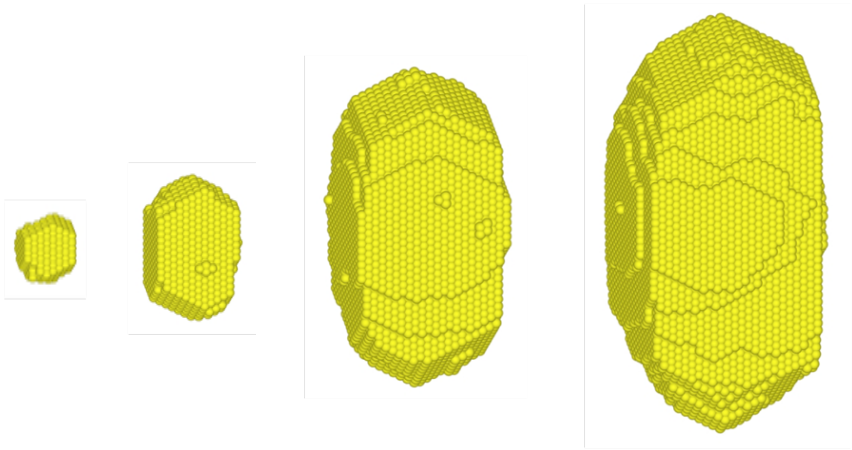

Figure 26: Snapshots of the simulation of deposition on a spherical PETN seed of 5 nm in diameter at 300 K. (a) after deposition of 2×10^2 molecules, (b) 2×10^3 molecules, (c) 1.5×10^4 molecules and (d) 3×10^4 molecules.

Controlling the ratio between the sizes of the 101 and 110 facets can be achieved by varying experimental conditions such as deposition rate and growth temperature. Experimental data suggest that at lower temperatures crystallites tend to be more round with a 110/101 aspect ratio being close to unity, while elevated temperatures tend to yield needle-like crystals [31]. Temperature clearly affects all the important kinetic processes, i.e., adsorption, desorption, and diffusion rates on each surface. Although we eventually plan on computing and

implementing the important rates into our MC, as a first approximation we decided to incorporate the temperature effects simply by varying the number of MC steps between insertions of new particles. Figures 27(a-d) show the resulting configurations following 3.5×10^4 particle insertions respectively at the rates of 10, 25, 50 and 100 MC diffusion steps between insertions. This variation can be interpreted either as an increase in surface diffusivity (e.g., by increasing the growth temperature) or as a decrease in growth rate. Therefore the progressively needle-like evolution in going from Fig. 27(a) to 27(d) is a clear manifestation of what is seen experimentally [31]. It is apparent that the results shown in Fig. 27 have little relationship to the equilibrium shape of the crystal shown in Fig. 25(b). To explain the long needle-like shapes based on equilibrium morphologies would require large ratios between the surface free energies; ratios corresponding to the aspect ratios of the crystal shapes. The wide variation in morphologies observed in real crystals of PETN is direct evidence of the predominance of kinetics in this system, even though these crystals are not formed under highly non-equilibrium conditions.

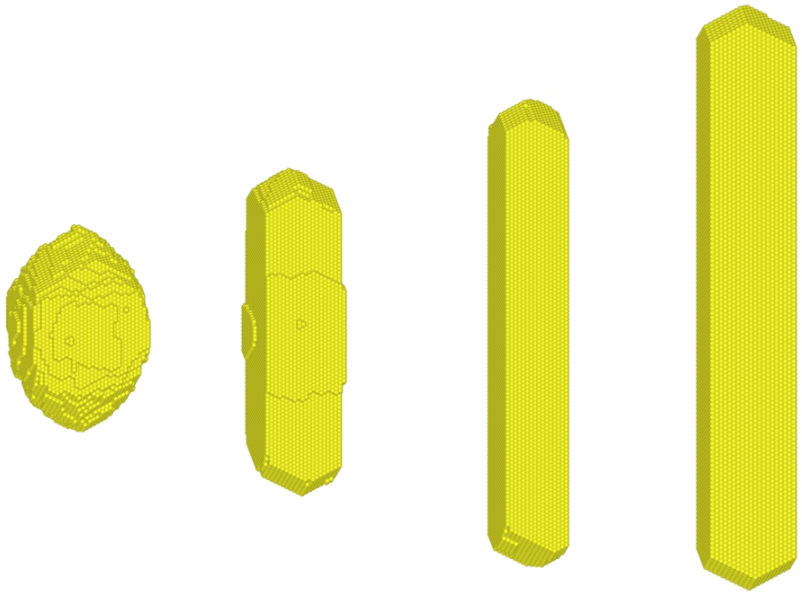

Figure 27: Comparison of the final configurations obtained after deposition of 3.5×10^4 particles on a spherical seed with (a) 10 MC steps, (b) 25 MC steps, (c) 50 MC steps, and (d) 100 MC steps between particle insertion.

The change in the morphology from the rounded shapes at low temperatures (few diffusion hops) to the anisotropic shapes at high temperatures can also be understood in terms of the surface diffusion occurring between molecule additions. If a molecule makes only a few diffusion hops before another molecule

arrives in its vicinity, then nucleation is favored by the high probability of the association of the two molecules into a small cluster. The high nucleation probability means that molecules are likely to stick close to the point where they originate, and the various crystal faces will advance at approximately the same rate. At high temperatures where the molecules execute a large number of diffusion hops between molecule additions, they diffuse over larger distances as a mobile unit before joining a surface cluster or encountering another molecule to form a new cluster. Some of the molecules will be able to diffuse across the surface of the crystallite to another facet. The exchange of molecules between facets will result in higher concentrations of mobile species on the facets where the potential energy is lower, and this will in turn result in a disparity in growth rates on the facets. Thus, the higher diffusion rates at high temperature result in large variations in the growth rates as a consequence of different rates of the nucleation of clusters on the faces. Equilibrium forms based on Wulf plots, where the anisotropies in surface free energies cause only a relative small variation in the facet sizes, cannot explain this kinetic effect.

Auspices

This work was performed under the auspices of the U.S. Department of Energy by Lawrence Livermore National Laboratory under Contract DE-AC52-07NA27344.

References

[1] J. G. Koomey, S. Berard, M. Sanchez, H. Wong, Implications of historical trends in the electrical efficiency of computing, IEEE Annals of the History of Computing 33 (3) (2011) 46–54. doi:http://doi.ieeecomputersociety.org/10.1109/MAHC.2010.28.

[2] D. E. Liddle, The Wider Impact of Moore's Law, IEEE Solid-state Circuits Newsletter 20 (2006) 28–30.

[3] G. E. Moore, Cramming More Components onto Integrated Circuits, Electronics 38 (8) (1965) 114–117. doi:10.1109/jproc.1998.658762.
URL `http://dx.doi.org/10.1109/jproc.1998.658762`

[4] G. H. Gilmer, P. Bennema, Simulation of crystal growth with surface diffusion, Journal of Applied Physics 43 (4) (1972) 1347–1360.

[5] F. F. Abraham, G. M. White, Computer simulation of vapor deposition on two-dimensional lattices, Journal of Applied Physics 41 (4) (1970) 1841–1849.

[6] A. A. Chernov, Growth of copolymer chains and mixed crystals - trial-and-error statistics, Soviet Physics Uspekhi 13 (1) (1970) 101–128.

[7] J. B. Adams, Z. Wang, Y. Li, Modeling cu thin film growth, Thin Solid Films 365 (2) (2000) 201 – 210. doi:http://dx.doi.org/10.1016/S0040-6090(99)01047-0.

[8] J. W. Evans, P. Thiel, M. C. Bartelt, Morphological evolution during epitaxial thin film growth: Formation of 2d islands and 3d mounds, Surface Science Reports 61 (1 - 2) (2006) 1 – 128.

[9] A. F. Voter, Interatomic potentials for atomistic simulations, MRS Bulletin 21.

[10] A. K. Bhuiyan, S. K. Dew, M. Stepanova, Controlled self-assembly of nanocrystalline arrays studied by 3d kinetic monte carlo modeling, Communications in Computational Physics 9.

[11] R. Akis, D. K. Ferry, C. B. Musgrave, Kinetic lattice monte carlo simulations of processes on the silicon (100) surface, Physica E: Low-dimensional Systems and Nanostructures 19 (1-2) (2003) 183 – 187, ¡ce:title¿Fourth International Symposium on Nanostructures and Mesoscopic Systems.

[12] D. P. Landau, S. Pal, Monte carlo simulation of simple models for thin film growth by {MBE}, Thin Solid Films 272 (2) (1996) 184 – 194.

[13] P. Zhang, X. Zheng, S. Wu, J. Liu, D. He, Kinetic monte carlo simulation of cu thin film growth, Vacuum 72 (4) (2004) 405 – 410.

[14] J. K. A., Computer modeling of atomic scale crystal growth processes, Journal of Crystal Growth 198-199, Part 1 (0) (1999) 1 – 9.

[15] K. H. Guenther, Microstructure of vapor-deposited optical coatings, Applied Optics 23 (21) (1984) 3806–3816.

[16] K. A. Jackson, G. H. Gilmer, D. E. Temkin, Monte carlo simulation of the rapid crystallization of bismuth-doped silicon, Phys. Rev. Lett. 75 (1995) 2530–2533.

[17] K. M. Beatty, K. A. Jackson, Monte carlo modeling of dopant segregation, Journal of Crystal Growth 271 (3 - 4) (2004) 495 – 512. doi:http://dx.doi.org/10.1016/j.jcrysgro.2004.07.074.

[18] S. Piana, M. Reyhani, J. D. Gale, Simulating micrometre-scale crystal growth from solution, Nature 438 (7064) (2005) 70–73.

[19] J. D. Gale, S. Piana, Three-dimensional kinetic monte carlo simulation of crystal growth from solution, Journal of Crystal Growth 294 (2006) 46–52.

[20] H.-C. Huang, G. H. Gilmer, T. D. de la Rubia, An atomistic simulator for thin film deposition in three dimensions, Journal of Applied Physics 84 (7) (1998) 3636–3649. doi:10.1063/1.368539.

[21] K. A. Jackson, Kinetic Processes: Crystal Growth, Diffusion, and Phase Transitions in Materials, WILEY-VCH Verlag, 2005. doi:10.1002/anie.200485247.

[22] A. Pimpinelli, J. Villain, Physics of Crystal Growth, Cambridge University Press, 1999.

[23] J. A. Sethian, Level Set Methods and Fast Marching Methods, Cambridge University Press, 1999.

[24] T. S. Cale, G. B. Raupp, T. H. Gandy, Ballistic transport-reaction prediction of film conformality in tetraethoxysilane O2 plasma enhanced deposition of silicon dioxide, Journal of Vacuum Science & Technology A 10 (4, 1) (1992) 1128–1134. doi:10.1116/1.578214.

[25] T. S. Cale, M. K. Jain, D. S. Taylor, R. L. Duffin, C. J. Tracy, Model for surface-diffusion of aluminum-(1.5-percent) copper during sputter deposition, Journal of Vacuum Science & Technology B 11 (2) (1993) 311–318. doi:10.1116/1.586676.

[26] D. Adalsteinnson, J. A. Sethian, A level set approach to a unified model for etching, deposition, and lithography .1. algorithms and 2-dimensional simulations, Journal of Computational Physics 120 (1) (1995) 128–144. doi:10.1006/jcph.1995.1153.

[27] J. L. Li, J. P. Mcvittie, J. Ferziger, K. C. Saraswat, J. Dong, Optimization of intermetal dielectric deposition module using simulation, Journal of Vacuum Science & Technology B 13 (4) (1995) 1867–1874, 2nd Topical Conference on Manufacturing Science and Technology, at the 41st National Symposium of the American-Vacuum-Society, Denver, CO, Oct 24-28, 1994.

[28] H. J. Frost, C. V. Thompson, D. T. Walton, Simulation of thin-film grain structures .1. grain-growth stagnation, Acta Metallurgica et Materialia 38 (8) (1990) 1455–1462. doi:10.1016/0956-7151(90)90114-V.

[29] Y. Yang, R. Johnson, H. Wadley, A Monte Carlo simulation of the physical vapor deposition of nickel, Acta Materialia 45 (4) (1997) 1455–1468. doi:10.1016/S1359-6454(96)00256-X.

[30] C. Y. Chang, S. S. M., ULSI Devices, Wiley, 1996.

[31] L. A. Zepeda-Ruiz, A. Maiti, R. Gee, G. H. Gilmer, B. L. Weeks, Size and habit evolution of PETN crystals - a lattice Monte Carlo study, Journal of Crystal Growth 291 (2) (2006) 461–467. doi:10.1016/j.jcrysgro.2006.02.052.

[32] J. D. Weeks, G. H. Gilmer, Pair approximation equations for interfaces and free surfaces in ising-model, Journal of Chemical Physics 63 (7) (1975) 3136–3143. doi:10.1063/1.431742.

[33] D. T. J. Hurle, Handbook of Crystal Growth. V.1, Fundamentals : transport and stability; V.2, Bulk crystal growth : growth mechanism and dynamics, Elsevier, Amsterdam, 1993.

[34] J. D. Weeks, G. H. Gilmer, H. J. Leamy, Structural transition in ising-model interface, Physical Review Letters 31 (8) (1973) 549–551. doi:10.1103/PhysRevLett.31.549.

[35] M. Polcik, L. Wilde, J. Haase, Partial order of the quasiliquid during surface melting of Al(110), Physical Review Letters 78 (3) (1997) 491–494.

[36] G. H. Gilmer, H.-C. Huang, T. D. de la Rubia, J. Dalla Torre, F. Baumann, Lattice Monte Carlo models of thin film deposition, Thin Solid Films 365 (2) (2000) 189–200.

[37] J. E. Rubio, M. Jaraiz, I. Martin-Bragado, J. M. Hernandez-Mangas, J. Barbolla, G. H. Gilmer, Atomistic monte carlo simulations of three-dimensional polycrystalline thin films, Journal of Applied Physics 94 (1) (2003) 163–168.

[38] G. Ehrlich, F. G. Hudda, Atomic view of surface self-diffusion - tungsten on tungsten, Journal of Chemical Physics 44 (3) (1966) 1039–&.

[39] R. L. Schwoebel, E. J. Shipsey, Step motion on crystal surfaces, Journal of Applied Physics 37 (10) (1966) 3682–&.

[40] J. Dalla Torre, G. H. Gilmer, M. D. Rouhani, Imperfect wetting of vapor-deposited thin films: Monte carlo simulations and nucleation model, Physical Review B 69 (2004) 195414. doi:10.1103/PhysRevB.69.195414.

[41] L. A. Zepeda-Ruiz, G. H. Gilmer, C. C. Walton, A. V. Hamza, E. Chason, Surface morphology evolution during sputter deposition of thin films: lattice monte carlo simulations, Journal of Crystal Growth 312 (8) (2010) 1183 – 1187, the 17th American Conference on Crystal Growth and Epitaxy/The 14th {US} Biennial Workshop on Organometallic Vapor Phase Epitaxy/The 6th International Workshop on Modeling in Crystal Growth.

[42] L. A. Zepeda-Ruiz, E. Chason, G. H. Gilmer, Y. Wang, H. Xu, A. Nikroo, A. V. Hamza, Understanding the relation between stress and surface morphology in sputtered films: Atomistic simulations and experiments, Applied Physics Letters 95 (15) (2009) 151910.

[43] J. A. Floro, C. V. Thompson, R. Carel, P. D. Bristowe, Competition between strain and interface energy during epitaxial grain-growth in Ag films on Ni(001), Journal of Materials Research 9 (9) (1994) 2411–2424.

[44] C. V. Thompson, R. Carel, Stress and grain growth in thin films, Journal of the Mechanics and Physics of Solids 44 (5) (1996) 657–673, Engineering Foundation Conference on Mechanics and Physics of Layered and Graded Materials, Davos, Switzerland, Aug 21-25, 1995.

[45] J. E. Greene, J. E. Sndgren, L. Hultman, I. Petrov, D. B. Bergstrom, Development of preferred orientation in polycrystalline tin layers grown by ultrahigh-vacuum reactive magnetron sputtering, Applied Physics Letters 67 (20) (1995) 2928–2930.

[46] P. Vogl, U. Hansen, V. Fiorentini, Multiscale approaches for metal thin film growth, Computational Materials Science 24 (1-2) (2002) 58 – 65.

[47] M. K. Sheergar, T. Smy, S. K. Dew, M. J. Brett, Simulation of threedimensional refractory metal step coverage over contact cuts and vias, Journal of Vacuum Science & Technology B 14 (4) (1996) 2595–2602.

[48] K. F. Jensen, S. T. Rodgers, R. Venkataramani, Multiscale modeling of thin film growth, Current Opinion in Solid State and Materials Science 3 (6) (1998) 562 – 569.

[49] J. W. Mullin, Crystallization, 4th Edition, Butterworth-Heinemann, Oxford, 2001.

[50] H. J. Scheel, F. T., Crystal Growth Technology, Wiley, 2003.

[51] A. Bravais, Etudes Crystallographiques, Acedemie des Sciences, Paris, 1913.

[52] J. D. H. Donnay, D. Harker, A new law of crystal morphology extending the law of bravais, American Mineralogist 22 (5) (1937) 446–467.

[53] J. W. Gibbs, The Collected Works, Longman, New York, 1928.

[54] P. Hartman, W. G. Perdok, On the relations between structure and morphology of crystals .1., Acta Crystallographics 8 (1) (1955) 49–52.

[55] R. Docherty, G. Clydesdale, K. J. Roberts, P. Benemma, Application of Bravais-Friedel-Donnay-Harker, attachement energy and ising-models to predicting and understanding the morphology of molecular-crystals, Journal of Physics D-Applied Physics 24 (2) (1991) 89–99.

[56] M. Brunsteiner, S. L. Price, Morphologies of organic crystals: Sensitivity of attachment energy predictions to the model intermolecular potential, Crystal Growth & Design 1 (6) (2001) 447–453.